Optics Letters

Ultrahigh-resolution optical vector analysis using fixed low-frequency electrical phase-magnitude detection

Min Xue, Wei Chen, Yuqing Heng, Ting Qing, and Shilong Pan*

Key Laboratory of Radar Imaging and Microwave Photonics, Ministry of Education, Nanjing University of Aeronautics and Astronautics, Nanjing 210016, China
Corresponding author: pans@nuaa.edu.cn

An ultrahigh-resolution optical vector analyzer (OVA) is proposed and experimentally demonstrated based on microwave photonic frequency downconversion and fixed low-frequency electrical phase-magnitude detection. In the proposed OVA, two optical single-sideband (OSSB) signals are generated by two RF signals with a fixed frequency spacing. One propagates through an optical device under test (DUT) and is then combined with the other before entering to a low-speed photodetector. By photodetection, a low-frequency and frequency-fixed photocurrent carrying the spectral responses is achieved. Hence, a low-frequency electrical phase-magnitude detector is sufficient to extract the magnitude and phase. Sweeping the frequency of the RF signals, the spectral responses of the DUT can be obtained. As compared with the conventional OSSB- and optical double-sideband-based OVA, the proposed OVA avoids the use of high-speed photodetection and broadband electrical phase-magnitude detection. In addition, it is inherently immune to the measurement errors induced by high-order sidebands and has the capability of measuring arbitrary spectral responses. In an experiment, the proposed OVA is implemented based on an electrical phase-magnitude detector working at 10 MHz. The measurement resolution is 1 MHz, and the measurement range is larger than 45 GHz. © 2018 Optical Society of America

Optical devices having the capability of finely manipulating the spectrum are of great importance in many emerging applications, such as optical single molecule detection [1], optical storage based on slow light [2], and on-chip optical signal processing [3]. To obtain the magnitude and phase spectral responses of these devices, optical vector analysis with ultrahigh resolution is required. One promising approach to perform the ultrahigh-resolution optical vector analysis is based on

microwave photonics (MWP), by which the optical spectral response analysis can be achieved in the electrical domain. Benefitting from the high-resolution and mature electrical techniques, the resolution can be improved thousands of times.

Generally, the MWP-based optical vector analyzers (OVAs) can be classified into two categories. The methods in the first category are implemented based on optical channel estimation (OCE), in which the magnitude and phase responses are achieved by comparing the optical orthogonal frequency-division multiplexing (OFDM) signals before and after an optical device under test (DUT) [4,5]. A resolution of 0.732 MHz was reported [4]. The OCE-based OVA can achieve one-shot measurement, but the dynamic range is usually small (e.g., 15 dB for a 5.86 MHz resolution [4]), because the severe intermodulation distortion in the electro-optic modulator limits the maximum input electrical power, leading to a low power spectral density for wideband signals. Moreover, the OCE-based method cannot be used to accurately characterize the nonlinear optical device, since the nonlinearity would significantly distort the spectrum of the OFDM signal. The other kind of MWP-based optical vector analysis is realized by electrical frequency sweeping and phase-magnitude detection. Optical single-sideband (OSSB) modulation [6–16] or optical double-sideband (ODSB) modulation [17–20] is usually applied to convert the electrical frequency sweeping to optical wavelength sweeping. A resolution as high as sub-hertz is potentially achievable in theory, and a 78 kHz resolution has been reported [6]. A key challenge associated with this kind of method is that high-speed photodetection and ultra-wideband (e.g., from 10 MHz to 67 GHz) electrical phase-magnitude detection are required, which makes the OVA complex, costly and, hence, difficult to construct. In addition, the nonlinearity in the electrical-to-optical and optical-to-electrical conversions would also introduce measurement errors and place a restriction on the dynamic range.

In this Letter, we propose and demonstrate an OSSB-based OVA using microwave photonic frequency downconversion and low-frequency and frequency-fixed electrical phase-magnitude detection. In the proposed OVA, two OSSB signals are used, which are generated by two RF signals with a fixed

frequency spacing of $\Delta\omega$. After propagating an OSSB signal through an optical DUT, a low-frequency photodetector (PD) receives the two OSSB signals and converts them into a photocurrent with a fixed frequency of $\Delta\omega$. Then a frequency-fixed and low-frequency electrical phase-magnitude detector is employed to extract the magnitude and phase information of the photocurrent. By sweeping the frequency of the two RF signals, the magnitude and phase responses of the DUT are thus achieved. Since the spectral responses are carried by a frequency-fixed and low-frequency photocurrent, the use of ultrawide electrical phase-magnitude detection is avoided. Moreover, the frequency of the frequency-fixed component (i.e., the $\Delta\omega$ component) has a frequency different from those beaten by other sidebands, so the measurement results are immune to the high-order-sideband-induced errors, which is a crucial problem for the conventional OSSB- and ODSB-based OVAs. As only one of the two OSSB signals goes through the optical DUT and the other OSSB signal will not be attenuated when measuring stopband responses, the proposed OVA has the capability of measuring arbitrary spectral responses. In a proof-of-concept experiment, the magnitude and phase responses of an optical Hilbert transformer are accurately measured with a resolution of 1 MHz by using an electrical phase-magnitude detector working at 10 MHz. In addition, the spectral responses from the stopband to the passband of an optical bandpass filter are successfully achieved, verifying the capability of measuring arbitrary spectral responses.

Figure 1 shows the schematic diagram of the proposed OSSB-based OVA achieved by microwave photonic frequency downconversion and fixed low-frequency electrical phase-magnitude detection. A tunable laser source (TLS) generates an optical carrier, which is then divided into two portions by an optical splitter (OS). The two optical signals are modulated by two RF signals with a fixed frequency spacing at two OSSB modulators. The optical fields of the two RF-modulated OSSB signals are

$$E_1(t) = \sum_n A_n \exp[i(\omega_o + n\omega_1)t], \tag{1}$$

$$E_2(t) = \sum_n B_n \exp[i(\omega_o + n\omega_2)t], \tag{2}$$

where ω_o, ω_1, and ω_2 are the angular frequencies of the optical carrier and the RF signals from two RF sources, respectively. A_n
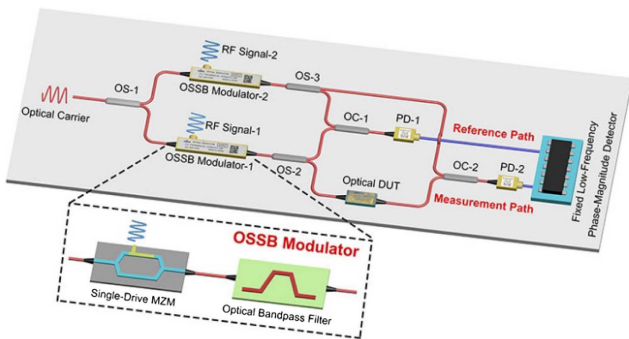
Fig. 1. Schematic diagram of the proposed OSSB-based OVA achieved by fixed low-frequency electrical phase-magnitude detection. OS, optical splitter; OSSB, optical single-sideband; MZM, Mach–Zehnder modulator; DUT, device under test; OC, optical coupler; PD, photodetector.

and B_n are the complex amplitude of the nth-order sidebands of the generated OSSB signals.

After propagating through an optical DUT, the magnitude and phase of the OSSB signal produced by the OSSB modulator-1 are changed according to the transmission function of the DUT. Hence, the propagated signal is

$$E_T(t) = A_{-1}H(\omega_o - \omega_1)\exp[i(\omega_o - \omega_1)t] + A_0 H(\omega_o)\exp(i\omega_o t)$$
$$+ A_{+1}H(\omega_o + \omega_1)\exp[i(\omega_o + \omega_1)t]$$
$$+ \sum_{\substack{n=-\infty \\ n\neq -1,0,1}}^{n=+\infty} A_n H(\omega_o + n\omega_1)\exp[i(\omega_o + n\omega_1)t], \tag{3}$$

where $H(\omega) = H_{\text{DUT}}(\omega) \cdot H_{\text{sys}}(\omega)$, $H_{\text{DUT}}(\omega)$ and $H_{\text{sys}}(\omega)$ are the transmission functions of the DUT and the measurement system, respectively. The propagated OSSB signal is then combined with the OSSB signal from the OSSB modulator-2, which is given by

$$E(t) = A_{-1}H(\omega_o - \omega_1)\exp[i(\omega_o - \omega_1)t] + B_{-1}\exp[i(\omega_o - \omega_2)t]$$
$$+ A_0 H(\omega_o)\exp(i\omega_o t) + B_0 \exp(i\omega_o t)$$
$$+ A_{+1}H(\omega_o + \omega_1)\exp[i(\omega_o + \omega_1)t]$$
$$+ B_{+1}\exp[i(\omega_o + \omega_2)t]$$
$$+ \sum_{\substack{n=-\infty \\ n\neq -1,0,1}}^{n=+\infty} A_n H[\omega_o + (n+1)\omega_1]\exp[i(\omega_o + n\omega_1)t]$$
$$+ \sum_{\substack{n=-\infty \\ n\neq -1,0,1}}^{n=+\infty} B_n \exp[i(\omega_o + n\omega_2)t]. \tag{4}$$

By square-law detection of (4) in a low-speed PD, the optical signal is converted into a photocurrent composed of plenty components with different frequencies. The transmission function information of the optical DUT is carried by the component with a frequency of $\Delta\omega = \omega_2 - \omega_1$ (assuming $\omega_2 > \omega_1$), which has a different frequency from the components generated by the high-order sidebands and the component produced by the two optical carriers. Then a fixed low-frequency electrical phase-magnitude detector working at $\Delta\omega$ is employed, which only receives the $\Delta\omega$-component and eliminates the components with different frequencies. Thus, the influence of the high-order sidebands and the optical carrier is eliminated, and the desired component is precisely received for extracting the magnitude and phase information, which is

$$i(\Delta\omega) = \eta A_{-1}B_{-1}^* H(\omega_o - \omega_1) + \eta A_{+1}^* B_{+1} H^*(\omega_o + \omega_1), \tag{5}$$

where η is the responsivity of the PD at $\Delta\omega$. On the right-hand of (5), the first term is the desired component which contains the frequency responses of the optical DUT, and the second term is the measurement error induced by the residual $+1$st-order sidebands. As the OSSB signals usually have the large sideband suppression ratios, which is typically over 30 dB (i.e., $|A_{-1}/A_{+1}| > 30$ dB, $|B_{-1}/B_{+1}| > 30$ dB), the power of the measurement error is much smaller than that of the desired component (typically over 60 dB), so the measurement errors are ignorable. Hence, (5) can be simplified as

$$i(\omega_1) = \eta A_{-1}B_{-1}^* H(\omega_o - \omega_1). \tag{6}$$

To eliminate the influence of the measurement system, such as uneven frequency responses, insert loss, responsivity, and so

on, a calibration process is performed. In this case, the DUT is removed, and the two test ports are directly connected, i.e., $H_{\text{DUT}}(\omega) = 1$. Thereby, the transmission function of the measurement system, i.e., $H_{\text{sys}}(\omega)$, can be acquired:

$$i_{\text{sys}}(\omega_1) = \eta A_{-1} B_{-1}^* H_{\text{sys}}(\omega_{\text{o}} - \omega_1). \tag{7}$$

From (6) and (7), we can obtain the accurate transmission function of the DUT, which can be written as

$$H_{\text{DUT}}(\omega_{\text{o}} + \omega_1) = \frac{i(\omega_1)}{i_{\text{sys}}(\omega_1)}. \tag{8}$$

Sweeping the frequencies of the RF sources with a fixed frequency spacing, the frequency responses of the DUT are obtained. As can be seen from (8), the transmission function of the DUT is obtained by detecting the fixed low-frequency component with a frequency of $\Delta\omega$.

An experiment based on the setup shown in Fig. 1 is performed. A lightwave with an optical power of 16 dBm is generated by a TLS (TeraXion Inc. PS-TNL), which is split into two parts and then sent to two OSSB modulators. The two optical signals are modulated by two RF signals with a frequency spacing of 10 MHz from an electrical vector network analyzer with the mixer measurement option (VNA, R&S ZVA67). The OSSB modulator is composed of a single-drive Mach–Zehnder modulator (MZM, Fujitsu FTM7938EZ) bias at the minimum transmission point and a tunable optical bandpass filter (Yenista XTM-50). A programmable optical filter (Finisar WaveShaper 4000s) serves as an optical DUT, which is set to achieve an optical Hilbert transformer and an optical bandpass filter. Two PDs are inserted to convert the optical signals into photocurrents. Referred by the photocurrent in the reference path, the electrical phase-magnitude detector working at 10 MHz in the VNA extracts the magnitude and phase of the photocurrent in the measurement path. The optical spectra are measured by a high-resolution optical spectrum analyzer (OSA, APEX AP2040C) with a resolution of 5 MHz.

Figure 2 shows the optical spectrum of the optical signal in the reference path when two RF signals having frequencies of 10 and 10.01 GHz are injected into the two OSSB modulators. As can be seen, the two +1st-order sidebands from the two OSSB modulators have a frequency spacing of 10 MHz, as shown in the inset of Fig. 2, which occupies the most power of the optical signal. The frequency spacing between the high-order sidebands is apparently different from that between the two +1st-order sidebands. For two nth-order sidebands, the frequency spacing is n times that between the two +1st-order sidebands. For a 10 MHz phase-magnitude detector, the components generated by the undesired sidebands, including the high-order sidebands and optical carrier, are filtered out and, thus, have no influence on the measurement results.
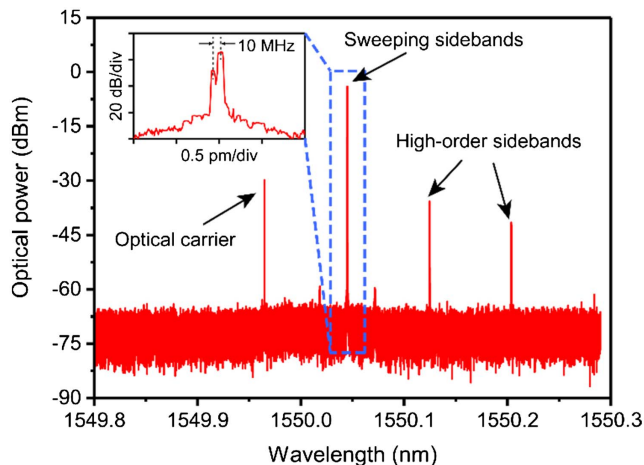
Figure 3 shows the magnitude and phase responses measured by the conventional and the proposed OSSB-based OVAs when the programmable optical filter is configured to have Hilbert transformation responses and services as the DUT. As can be seen, the magnitude and phase responses of the DUT in a frequency range of 30 GHz (10–40 GHz offset the optical carrier) are measured (red solid lines). There are 30001 measurement points during the measurement range corresponding to a resolution of 1 MHz, which can be improved by increasing the points. A resolution of 10 kHz is available for the implemented measurement system, which is restricted by the linewidth of the TLS (<10 kHz). By employing a sub-hertz-linewidth laser [21], a resolution as high as hertz level is potentially achievable in theory. It is worth mentioning that, limited by the lowest working frequency of the VNA (i.e., 10 MHz), the frequency spacing between the two RF signals is correspondingly set to 10 MHz. An electrical phase-magnitude detector that has lower working frequency can also be used. Theoretically, the lowest working frequency is limited by the linewidth of the laser source.

As a comparison, the optical DUT is also characterized by the conventional OSSB-based OVA. The measured magnitude and phase responses are plotted in Fig. 3 (blue dashed lines). As can be seen, the frequency responses measured by the two methods agree well. A 180 deg phase shift, as well as a notch, appears around 22.5 GHz. It should be noted that the frequency responses measured by the proposed method are slightly different from those measured by the conventional OSSB-based OVAs. This is because the optical signal to

Fig. 2. Optical spectrum of the optical signal sent to the PD in the reference path.
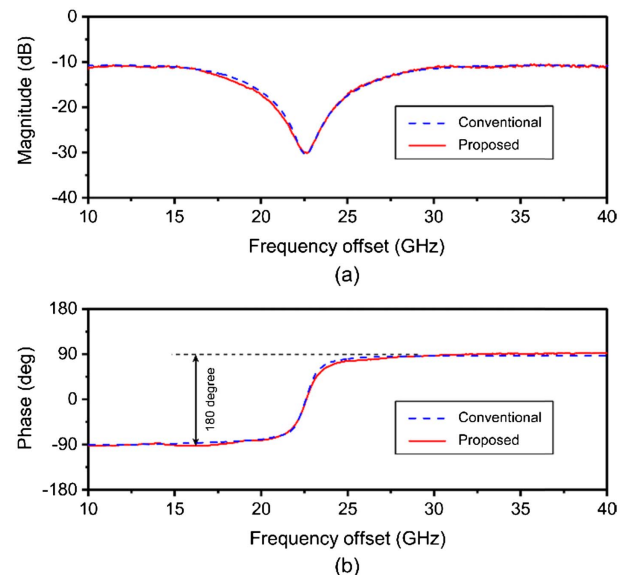
Fig. 3. (a) Magnitude and (b) phase responses measured by the conventional and proposed OSSB-based OVAs.
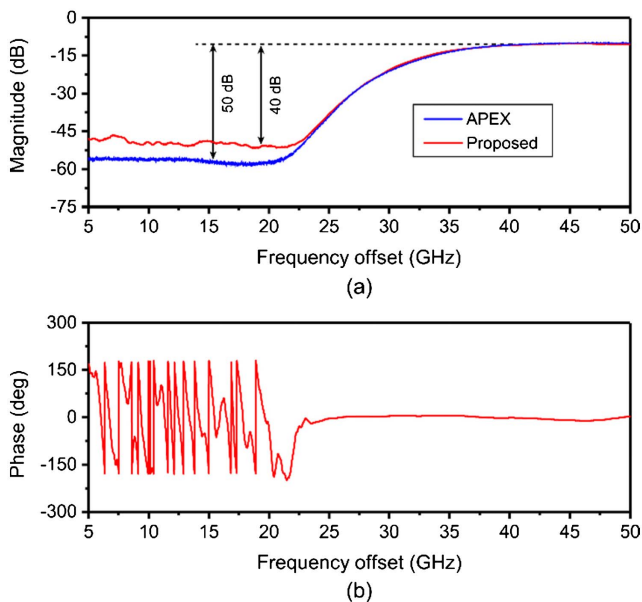
Fig. 4. Measured (a) magnitude and (b) phase responses of the optical bandpass filter.

generate the photocurrent is from the two separated optical paths in the proposed method, where the mechanical vibrations and thermal fluctuations have an influence on the stability of the measurement system. By carefully controlling temperature and isolating vibration, the improved measurement results are achievable.

Another advantage of the proposed method is the capability of measuring the arbitrary responses. The bandpass responses, which are difficult to measure by the conventional OSSB-based OVA, are measurable. Figure 4 shows the measured magnitude and phase responses around the rising edge of the bandpass filter configured by the programmable optical filter (red lines). As can be seen, the bandpass responses in a frequency range of 45 GHz (5–50 GHz offset the optical carrier) are measured from stopband to passband, which is unachievable for the conventional OSSB- and ODSB- based OVAs, since the optical carrier would be significantly suppressed by the stopband, and no photocurrent would be produced. The magnitude response measured by a high-resolution OSA (APEX AP2040C) with the optical component analysis option is also plotted in Fig. 4(a) (blue line). As can be seen, the magnitude responses measured by the two methods are coincident at the passband and the rejecting skirt. Since the commercial instrument achieves the spectral responses by directly measuring the optical powers before and after the DUT, it observes larger suppression of the stopband, but only the magnitude responses can be obtained. The rejection ratios between the passband and the stopband measured by the proposed method and the commercial instrument are about 40 and 50 dB, respectively. The magnitude response of the stopband measured by the proposed method shows that the measurable loss is about 45 dB. Considering that a 30 dB gain is also measurable, the dynamic range of the measurement system is over 75 dB.

In conclusion, an ultrahigh-resolution OVA achieved by fixed low-frequency electrical phase-magnitude detection is proposed and experimentally demonstrated. Thanks to the high-performance MWP-based frequency downconversion, the high-speed photodetection and the ultra-wideband electrical phase-magnitude detection, which are the essential components for the previous MWP-based OVAs, are omitted. In addition, the proposed OVA is immune to the high-order-sideband-induced errors and has the capability of measuring the arbitrary spectral responses. The spectral responses of an optical Hilbert transformer and an optical bandpass filter achieved by a programmable optical filter are experimentally measured when the phase-magnitude detector works at 10 MHz. Since the photocurrent is generated by two optical signals from two separated optical paths, the proposed OVA is sensitive to the environment. To achieve the accurate measurement results, temperature should be controlled, and the vibration should be isolated.

REFERENCES

1. M. D. Baaske, M. R. Foreman, and F. Vollmer, Nat. Nanotechnol. **9**, 933 (2014).
2. C. H. Dong, Z. Shen, C. L. Zou, Y. L. Zhang, W. Fu, and G. C. Guo, Nat. Commun. **6**, 6193 (2015).
3. R. Pant, D. Marpaung, I. V. Kabakova, B. Morrison, C. G. Poulton, and B. J. Eggleton, Laser Photon. Rev. **8**, 653 (2014).
4. X. W. Yi, Z. H. Li, Y. Bao, and K. Qiu, IEEE Photon. Technol. Lett. **24**, 443 (2012).
5. C. Jin, Y. Bao, Z. Li, T. Gui, H. Shang, X. Feng, J. Li, X. Yi, C. Yu, G. Li, and C. Lu, Opt. Lett. **38**, 2314 (2013).
6. S. Pan and M. Xue, J. Lightwave Technol. **35**, 836 (2017).
7. J. E. Román, M. Y. Frankel, and R. D. Esman, Opt. Lett. **23**, 939 (1998).
8. Z. Z. Tang, S. L. Pan, and J. P. Yao, Opt. Express **20**, 6555 (2012).
9. M. Sagues, M. Pérez, and A. Loayssa, Opt. Express **16**, 16181 (2008).
10. M. Sagues and A. Loayssa, Opt. Express **18**, 17555 (2010).
11. W. Li, W. T. Wang, L. X. Wang, and N. H. Zhu, IEEE Photon. J. **6**, 7901108 (2014).
12. W. T. Wang, W. Li, J. G. Liu, W. H. Sun, W. Y. Wang, and N. H. Zhu, IEEE Photon. J. **6**, 5501310 (2014).
13. M. Xue, S. L. Pan, and Y. J. Zhao, Opt. Lett. **40**, 569 (2015).
14. M. Wang and J. P. Yao, IEEE Photon. Technol. Lett. **25**, 753 (2013).
15. S. Song, X. Yi, S. X. Chew, L. Li, L. Nguyen, and R. Minasian, *IEEE International Topical Meeting on Microwave Photonics* (2016), pp. 98–101.
16. L. Li, X. Yi, S. X. Chew, S. Song, L. Nguyen, and R. Minasian, *22nd International Conference on Applied Electromagnetics and Communications (ICECOM)* (2016), pp. 1–4.
17. W. Jun, L. Wang, C. Yang, M. Li, N. H. Zhu, J. Guo, L. Xiong, and W. Li, Opt. Lett. **42**, 4426 (2017).
18. M. Xue, S. F. Liu, and S. L. Pan, IEEE Photon. Technol. Lett. **30**, 491 (2018).
19. S. F. Liu, M. Xue, J. B. Fu, L. G. Wu, and S. L. Pan, Opt. Lett. **43**, 727 (2018).
20. T. Qing, S. P. Li, M. Xue, W. Li, N. H. Zhu, and S. L. Pan, Opt. Express **25**, 4665 (2017).
21. T. Kessler, C. Hagemann, C. Grebing, T. Legero, U. Sterr, F. Riehle, M. J. Martin, L. Chen, and J. Ye, Nat. Photonics **6**, 687 (2012).